

LANDAU THEORY FOR SHAPE MEMORY POLYCRYSTALS

R. Ahluwalia, T. Lookman, A. Saxena, and R.C. Albers

Theoretical Division, Los Alamos National Laboratory,

Los Alamos, New Mexico, 87545 USA

(Dated: October 24, 2018)

Abstract

We propose a Ginzburg-Landau theory for the elastic properties of shape memory polycrystals. A single crystal elastic free energy for a system that undergoes a square-to-rectangle transformation is generalized to a polycrystal by introducing a crystal orientational field that is determined from a continuum phase field model. The coupled system is used to study domain morphology and mechanical properties of shape memory alloys in different temperature regimes.

KEYWORDS: Shape Memory, Martensites, Polycrystals, Stress-Strain response, Landau theory.

PACS numbers:

I. INTRODUCTION

Materials known as martensites undergo first-order, diffusionless structural transformations from one crystal phase (austenite) to another, usually a twinned, phase (martensite) due to shear strains. A subclass of these materials with displacive transformations exhibits the shape memory effect¹. This effect refers to the existence of a residual strain upon unloading that can be recovered on heating to the high temperature austenite phase. In the austenite phase, these materials exhibit pseudoelastic behavior where a plateau in the stress-strain curves is observed; however, there is no residual strain as the macroscopic deformation is completely recovered when the load is removed. Interestingly, these unusual mechanical properties of shape memory alloys do not involve any plastic effects such as those caused by dislocation motion but are entirely due to the intrinsic elastic nonlinearities. As a consequence of these unique properties, shape memory materials have many technological applications². Some examples include NiTi, FePd, AuCd and copper-based ternary alloys, e.g. CuAuZn.

Most commercial applications of shape memory alloys make use of polycrystalline specimens and therefore it is important to compare the mechanical response of polycrystals to that of single crystals. The problem of finding the effective properties of martensitic polycrystals has been studied by analytical methods^{3,4,5} and finite element simulations⁶. However, these methods do not account for the complex polycrystal geometry and also do not incorporate the long-range elastic interactions between the grains. Continuum simulations that span a range of length scales are good candidates to describe these issues. Recently, phase-field micro-elasticity models that employ static grains created by the Voronoi construction have been studied⁷. However, it is important to regard the grain orientation as a thermodynamic variable since a polycrystal, in reality, is a metastable state that is formed by a grain growth process. In the present work, we attempt to account for this metastability of a polycrystal.

The evolution of grains during grain growth has been studied using the phase-field approach^{8,9,10}. Although these models correctly describe the grain morphologies and domain coarsening, they do not address the issues of elasticity and crystal symmetry. A coupling of these models with continuum elasticity models of martensitic transformations provides a framework to model mechanical properties of shape memory polycrystals. Here we propose a model in which elastic strains are coupled to a phase-field model through an orientation field that is determined from a multi-component order parameter describing the crystal orientations. Due to this cou-

pling, the strains as well as the grain orientations can change under an external load. In Section 2 we describe our Ginzburg-Landau model and present two-dimensional ($2D$) simulations of the loading-unloading cycle for martensitic polycrystals in different temperature regimes in Section 3. Our main findings are summarized in section 4.

II. GINZBURG-LANDAU MODEL

A Landau theory for shape memory materials was first proposed by Falk¹¹. This one dimensional model captures the salient physics of a number of experimentally observed features of martensites. However, the model does not incorporate the elastic long-range interactions that are crucial to describe the microstructure of martensites. Barsch and Krumhansl introduced a Ginzburg-Landau model to describe the inhomogeneous microstructure of these materials¹² and the model has been extended to simulate martensitic domain structures in two and three dimensions^{13,14,15,16,17}. Here we generalize this theory to describe a $2D$ square to rectangle martensitic transformation in a polycrystal with different crystallographic orientations. The theory is formulated in terms of a free-energy functional

$$F = \int d\vec{r} [f_{grain} + f_{elastic} + f_{load}], \quad (1)$$

where f_{grain} is the free energy density due to the orientational degrees of freedom of the polycrystal, $f_{elastic}$ represents the elastic free energy and f_{load} is the free energy contribution due to an external applied load. The polycrystalline system is described by a set of Q non-conserved order parameters⁹ ($\eta_1, \eta_2, \dots, \eta_Q$). In terms of these order parameters the free energy f_{grain} is given by

$$f_{grain} = \sum_{i=1}^Q \left[\frac{a_1}{2} \eta_i^2 + \frac{a_2}{3} \eta_i^3 + \frac{a_3}{4} \eta_i^4 \right] + \frac{a_4}{2} \sum_{i=1}^Q \sum_{j>i} \eta_i^2 \eta_j^2 + \sum_{i=1}^Q \frac{K}{2} (\nabla \eta_i)^2. \quad (2)$$

For $a_1, a_2 < 0$ and $a_3, a_4 > 0$, the first two terms in equation (2) describe a potential with Q degenerate minima $(\eta_0, 0, \dots, 0)$, $(0, \eta_0, \dots, 0)$ up to $(0, 0, \dots, \eta_0)$ ($\eta_0 > 0$), corresponding to Q grain orientations. This form differs from that used by Chen and Yang⁹ as there is an additional cubic term in the free energy. The cubic term ensures that $\eta_0 \geq 0$ and allows us to uniquely associate an orientation with each minimum, given by an angle

$$\theta(\vec{\eta}, \vec{r}) = \frac{\theta_m}{Q-1} \left[\frac{\sum_{i=1}^Q i \eta_i(\vec{r})}{\sum_{i=1}^Q \eta_i(\vec{r})} - 1 \right]. \quad (3)$$

Thus, there are Q orientations between 0 and a maximum angle θ_m (as an example, the $Q = 3$ case has minima at $(\eta_0, 0, 0)$ and $(0, \eta_0, 0)$ and $(0, 0, \eta_0)$ corresponding to $\theta = 0^\circ$, $\theta = \theta_m/2$ and $\theta = \theta_m$).

The gradient energy ($K > 0$) represents the energy cost of creating a grain boundary. To describe elastic effects, we consider the linearized strain tensor in a global reference frame defined as $\epsilon_{ij} = (u_{ij} + u_{ji})/2$ ($i = 1, 2; j = 1, 2$), where u_i represents a component of the displacement vector and u_{ij} is a displacement gradient. We use the symmetry-adapted linear combinations of the strain tensor¹² defined by $\epsilon_1 = (\epsilon_{xx} + \epsilon_{yy})/\sqrt{2}$, $\epsilon_2 = (\epsilon_{xx} - \epsilon_{yy})/\sqrt{2}$ and $\epsilon_3 = \epsilon_{xy}$. Here ϵ_1 represents the bulk (dilatation) strain, ϵ_2 the deviatoric (rectangular) strain and ϵ_3 the shear strain. To generalize these definitions to the case of a polycrystal described by an orientational field $\theta(\vec{\eta})$, the strain tensor in a rotated frame is calculated using $R(\theta(\vec{\eta})) \overset{\leftrightarrow}{\epsilon} R^T(\theta(\vec{\eta}))$, where $R(\theta(\vec{\eta}))$ is a rotation matrix and $\theta(\vec{\eta})$ is determined from the minima of F_{grain} using equation (3). Under this rotation, the elastic free energy describing a square to rectangle transition is given by

$$f_{elastic} = \frac{A_1}{2}e_1^2 + \frac{A_3}{2}e_3^2 + f_{local}(e_2) + \frac{K_2}{2}(\nabla e_2)^2, \quad (4)$$

where $e_1 = \epsilon_1$, $e_2 = \epsilon_2 \cos[2\theta(\vec{\eta})] + \sqrt{2}\epsilon_3 \sin[2\theta(\vec{\eta})]$ and $e_3 = -(1/\sqrt{2})\epsilon_2 \sin[2\theta(\vec{\eta})] + \epsilon_3 \cos[2\theta(\vec{\eta})]$. The nonlinear part of the elastic free energy is

$$f_{local}(e_2) = \frac{A_2}{2}e_2^2 + \frac{\alpha}{4}e_2^4 + \frac{\beta}{6}e_2^6. \quad (5)$$

At the level of the unit cell, the transformation free energy f_{local} describes a square to rectangle transition where the austenite phase (square) has $e_2 = 0$ and the martensite phase is described by $e_2 = \pm e_0$ corresponding to the two rectangular variants. Here $A_1 = C_{11} + C_{12}$, $A_2 = C_{11} - C_{12}$ and $A_3 = 4C_{44}$, where C_{11} , C_{12} and C_{44} are the elastic constants for a crystal with square symmetry. The quantities α and β are the higher order nonlinear elastic constants and K_2 is the appropriate deviatoric strain gradient coefficient that determines the energy cost of creating a domain wall (twin boundary) between the two rectangular variants. In principle, K_2 can be determined experimentally from phonon dispersion curves¹⁷. In this work, we are interested in simulating a uniaxial loading experiment. If we choose the x axis to be the loading axis, then the free energy contribution due to the external load σ is given by

$$\begin{aligned} f_{load} &= -\sigma\epsilon_{xx} = -\frac{\sigma}{\sqrt{2}}(\epsilon_1 + \epsilon_2) \\ &= -\frac{\sigma}{\sqrt{2}} \left[e_1 + e_2 \cos[2\theta(\vec{\eta})] - \sqrt{2}e_3 \sin[2\theta(\vec{\eta})] \right]. \end{aligned} \quad (6)$$

The strains ϵ_1 , ϵ_2 and ϵ_3 are not independent but are related by the elastic compatibility relation¹⁸

$$\nabla^2 \epsilon_1 - \left(\frac{\partial^2}{\partial x^2} - \frac{\partial^2}{\partial y^2} \right) \epsilon_2 - \sqrt{8} \frac{\partial^2}{\partial x \partial y} \epsilon_3 = 0. \quad (7)$$

In terms of the strain variables e_1 , e_2 and e_3 , this relation becomes

$$\begin{aligned} \nabla^2 e_1 - \left(\frac{\partial^2}{\partial x^2} - \frac{\partial^2}{\partial y^2} \right) \left[e_2 \cos[2\theta(\vec{\eta})] - \sqrt{2} e_3 \sin[2\theta(\vec{\eta})] \right] \\ - \sqrt{8} \frac{\partial^2}{\partial x \partial y} \left[\frac{e_2}{\sqrt{2}} \sin[2\theta(\vec{\eta})] + e_3 \cos[2\theta(\vec{\eta})] \right] = 0. \end{aligned} \quad (8)$$

We eliminate the strain e_1 from $f_{elastic}$ and f_{load} using equation (8) so that the total elastic energy is in terms of e_2 and e_3 only. This method has been used previously in the context of martensitic transformations in single crystals¹⁵. We first introduce $e'_1 = e_1 - (\sigma/A_1\sqrt{2})$ so that $f_{eff} = f_{elastic} + f_{load}$, where

$$f_{eff} = \frac{A_1}{2} e_1'^2 + \frac{A_3}{2} e_3^2 + f_{local}(e_2) - \frac{\sigma}{\sqrt{2}} \left[e_2 \cos[2\theta(\vec{\eta})] - \sqrt{2} e_3 \sin[2\theta(\vec{\eta})] \right]. \quad (9)$$

To eliminate e'_1 from equation (9), we use the Fourier representation of equation (8) to obtain

$$e'_1(\vec{k}) = \frac{k_x^2 - k_y^2}{k_x^2 + k_y^2} \Gamma_2(\vec{k}) + \frac{\sqrt{8} k_x k_y}{k_x^2 + k_y^2} \Gamma_3(\vec{k}), \quad (10)$$

where $\Gamma_2(\vec{k})$ represents the Fourier transform of $e_2 \cos[2\theta(\vec{\eta})] - \sqrt{2} e_3 \sin[2\theta(\vec{\eta})]$ and $\Gamma_3(\vec{k})$ is the Fourier transform of $e_2(\sin[2\theta(\vec{\eta})]/\sqrt{2}) + e_3 \cos[2\theta(\vec{\eta})]$. Thus, the effective free energy can be written as

$$\begin{aligned} F_{eff} = \frac{A_1}{2} \int d\vec{k} \left[\left(\frac{k_x^2 - k_y^2}{k_x^2 + k_y^2} \right)^2 |\Gamma_2(\vec{k})|^2 + \left(\frac{\sqrt{8} k_x k_y}{k_x^2 + k_y^2} \right)^2 |\Gamma_3(\vec{k})|^2 \right. \\ \left. + \frac{\sqrt{8} k_x k_y (k_x^2 - k_y^2)}{(k_x^2 + k_y^2)^2} \left(\Gamma_3(\vec{k}) \Gamma_2(-\vec{k}) + \Gamma_3(-\vec{k}) \Gamma_2(\vec{k}) \right) \right] \\ + \int d\vec{r} \left[\frac{A_3}{2} e_3^2 + f_{local}(e_2) - \frac{\sigma}{\sqrt{2}} \left(e_2 \cos[2\theta(\vec{\eta})] - \sqrt{2} e_3 \sin[2\theta(\vec{\eta})] \right) \right]. \end{aligned} \quad (11)$$

The long-range part of the free energy is always orientation dependent due to the elastic compatibility induced anisotropy in the kernels. This term ensures that elastic compatibility will be satisfied within the grains as well as at the grain boundaries. We emphasize that the long-range interaction excludes the $|\vec{k}| = 0$ mode since compatibility is trivially satisfied for this case. The $|\vec{k}| = 0$ mode, which refers to the homogeneous state, is accounted for by the local terms in F_{eff} . The total free energy of the system is $F = F_{grain} + F_{eff}$, and we assume relaxational dynamics

for e_2 and e_3 , that is,

$$\begin{aligned}\frac{\partial e_2}{\partial t} &= -\gamma_2 \left[\frac{\delta F}{\delta e_2} \right], \\ \frac{\partial e_3}{\partial t} &= -\gamma_3 \left[\frac{\delta F}{\delta e_3} \right],\end{aligned}\tag{12}$$

where γ_2 and γ_3 are the appropriate kinetic coefficients for the deviatoric and shear strains. Similarly, the dynamics of the grains is defined by Q equations

$$\frac{\partial \eta_i}{\partial t} = -\gamma_\eta \frac{\delta F}{\delta \eta_i},\tag{13}$$

where γ_η is a kinetic coefficient and $i = 1, \dots, Q$, corresponding to Q grain orientations.

III. SIMULATIONS OF TEXTURE AND STRAIN EVOLUTION

We simulate the mechanical properties of shape memory materials using the model described in Section 2. We choose FePd parameters¹⁷ for which $A_1 = 140$ GPa, $A_3 = 280$ GPa, $\alpha = -1.7 \times 10^4$ GPa and $\beta = 3 \times 10^7$ GPa. The temperature dependent elastic constant A_2 undergoes a softening and hence controls the square to rectangle transformation. We study four different cases corresponding to $A_2 = -2, 1, 2, 3$ GPa. Muto et al.¹⁹ have measured the elastic constants of FePd as a function of temperature. The lowest temperature measurement they reported was at 290 K corresponding to $A_2 \sim 10$ GPa. Thus the values of A_2 we have chosen correspond to temperatures lower than 290 K and are in the vicinity of the transition temperature of 265 K. Figure 1 shows the profiles for the free energy f_{local} for these values. For the parameters in f_{grain} we choose (for illustrative purposes) $a_1 = -10$ GPa, $a_2 = -10$ GPa, $a_3 = 10$ GPa, $a_4 = 20$ GPa, $Q = 5$ and $\theta_m = 30^\circ$. Here, we also need to specify the grain boundary energy coefficient K and the strain gradient coefficient K_2 . For FePd, the strain gradient coefficient¹⁷ has been measured to be $K_2/a_0^2 = 25$ GPa, where a_0 is the lattice spacing of the crystal. The grain boundary energy coefficient is chosen as $K/a_0^2 = 10^5$ GPa. The lengths are scaled by $\vec{r} = (100a_0)\vec{\zeta}$. For a homogeneous single crystal, using these parameter values, the free energy in equation (2) has 5 degenerate minima defined by $\theta_0(\vec{\eta}) = 0^\circ, 7.5^\circ, 15^\circ, 22.5^\circ, 30^\circ$. We should point out that we can consider a more continuous orientation distribution of the polycrystal with a large number of states (large value of Q) in the full range ($0^\circ - 45^\circ$). However, for the sake of clarity of the domain patterns, we restrict ourselves to the range described above. Equations (12) and (13) are solved

numerically to simulate the domain structures and mechanical properties in different regimes. For simplicity, we assume $\gamma_\eta = \gamma_2 = \gamma_3 = \gamma$ and use rescaled time defined by $t^* = t(10^{10}\gamma)$.

An initial polycrystalline configuration is first generated by solving equations (12) and (13) for a $12800a_0 \times 12800a_0$ system with periodic boundary conditions, starting from random initial conditions. A grain growth process is simulated with $\sigma = 0$ in the austenite phase so that all components of the strain tensor vanish. Grains with orientations $\theta_0(\vec{\eta}) = 0^\circ, 7.5^\circ, 15^\circ, 22.5^\circ, 30^\circ$ form and start coarsening. We arrest the system in a given polycrystalline configuration by abruptly changing the value of the parameter a_1 from -10 GPa to -160 GPa (the parameter A_2 is also changed so that the system is in the desired martensitic phase). This sudden decrease in a_1 increases the free energy barriers between the crystalline states and the growth stops. We first consider the case $A_2 = -2$ GPa. Figure 1 shows that for a homogeneous system, the transformation free energy $f_{local}(e_2)$ for $A_2 = -2$ GPa has a local maximum at $e_2 = 0$ and two degenerate global minima. In the absence of applied stress ($\sigma = 0$), the arrested polycrystal evolves into a domain pattern of the variants of the martensitic phase (there is no austenite present since $e_2 = 0$ is unstable). The strains in each grain as well as the orientation of the martensitic domain walls (i.e. twin boundaries) are determined by the orientation of the grain. This behavior is clear from Figure 2(a) that shows the distribution of the strain $\epsilon_2(\vec{r})$ (deviatoric strain relative to the global frame of reference) and Figure 2(b) that shows the local orientation $\theta(\vec{\eta}(\vec{r}))$. The domain walls are oriented at angles $\theta(\vec{\eta}) + \pi/4$ or $\theta(\vec{\eta}) - \pi/4$. We point out that the average strains for this configuration are very small and correspond to a system with no macroscopic deformation.

To simulate mechanical loading, an external tensile stress σ is applied quasi-statically, i.e., starting from the unstressed configuration of Figures 2(a) and 2(b), the applied stress σ is increased in steps of 5.13 MPa, after allowing the configurations to relax for $t^* = 25$ time steps after each increment. The loading is continued till a maximum stress of $\sigma = 200$ MPa is reached. Thereafter, the system is unloaded by decreasing σ to zero at the same rate at which it was loaded. Figures 2(c) and 2(d) relate to a stress level of $\sigma = 46.15$ MPa during the loading process. The favored variants (red domains in the left panel) have started to grow at the expense of the unfavored variants (blue domains in the left panel). The orientation distribution $\theta(\vec{\eta}(\vec{r}))$ in Figure 2(d) has not changed much. As the stress level is increased further, the favored variants grow. Even at the maximum stress of 200 MPa, some unfavored variants persist, as is clear from Figure 2(e) (in fact, further application of stress does not remove such structures as the unfavored variants are in a ‘‘locked’’ state due to intergranular constraints). We note that the grains with large misorientation with the

loading direction rotate, as is clear by comparing Figure 2(f) with Figure 2(b) and Figure 2(d), where we can observe that dark red colored grains have turned orange, indicating rotation of those grains. Grains with lower misorientation do not undergo significant rotation. This rotation is due to the tendency of the system to maximize the transformation strain in the direction of loading so that the total free energy is minimized. Within the grains that rotate, sub-grain bands with slightly higher values of the orientation $\theta(\vec{\eta}(\vec{r}))$ are present. These bands correspond to the unfavored strain variants that still survive. Figure 2(g) and 2(h) show the situation after unloading to $\sigma = 0$. Upon removing the load, a domain structure is nucleated again due to the local strain gradients at the grain boundaries and the surviving unfavored variants in the loaded polycrystal configuration in Figure 2(e). This domain structure is not the same as that prior to loading (Figure 2(a)) and thus there is an underlying hysteresis. The unloaded configuration has non-zero average strain. This average strain is recovered by heating to the austenite phase, as per the shape memory effect. Figure 2(h) shows that the orientation distribution reverts to its preloading state as the grains rotate back when the load is removed. To show the rotation of grains more clearly, we plot in Figure 3 the change in orientation $\Delta\theta = \theta(\sigma) - \theta(\sigma = 0)$ for $\sigma = 200$ MPa. It is clear by comparing this figure with Figure 2(b) that only grains with large misorientations with the loading axis ($\theta = 0^\circ$) rotate in order to decrease the misorientation. In some of these rotating grains, we observe bands where the misorientation has increased. As discussed earlier, these bands correspond to regions where the unfavored variants do not disappear even at high stresses. This behavior is a consequence of the intergranular constraints.

We compare the above mechanical behavior of the polycrystal to the corresponding single crystal. A single crystal simulation is set up with exactly the same elastic free energy parameters as the polycrystal case but the orientation is fixed at $\theta = 0^\circ$. Loading conditions are also identical to the polycrystal case. Figure 4 shows the evolution of the martensitic variants during the loading-unloading cycle for the single crystal. Figure 4(a), shows the simulated microstructure ($12800a_0 \times 12800a_0$) prior to loading, with domain wall orientations at $\pi/4$ or $-\pi/4$ everywhere. In contrast, the domain wall orientations change from grain to grain in the polycrystal case depicted in Figure 2(a). Figure 4(b) shows the domain patterns for a stress $\sigma = 46.15$ MPa. We see that the favored variants (red domains) grow at the expense of the unfavored variants (blue domains). This growth continues, as shown in Figure 4(c) ($\sigma = 56.41$ MPa) and Figure 4(d) ($\sigma = 71.79$ MPa). Finally, in Figure 4(e) ($\sigma = 200$ MPa) all unfavored variants disappear and we obtain a single domain, in contrast to the polycrystal case at the same stress level (Figure 2(e)) where unfavored

vored variants persist. Upon unloading, the single crystal remains in a single domain state (Figure 4(f)). This is because there are no inhomogeneities or thermal noise in the simulations to cause renucleation of the domain structure and so the system remains in the positive strain minimum homogeneously. The unloaded polycrystal, however, reverts to the domain pattern (Figure 2(g)). This also shows that, unlike the single crystal case, the mechanical behavior of the polycrystal is not necessarily governed by $f_{local}(e_2)$ but by a more complex inhomogeneous free energy landscape. A consequence of this is that the residual strain for a single crystal²⁰ will be larger than that for a polycrystal²¹. The stress-strain curves corresponding to Figure 2 and Figure 4 are shown in Figure 5. The residual strain for the polycrystal ($\sim 0.7\%$) is smaller than that for the single crystal ($\sim 1.8\%$) due to an effective averaging over different orientations and nucleation of domains at grain boundaries upon unloading. Also, the change in the stress-strain curve for the polycrystal is not abrupt because the response of the polycrystal is averaged over all grain orientations.

We now discuss cases where the material exists in the austenite phase prior to loading. As can be seen in Figure 1, $A_2 = 1, 2$ and 3 GPa correspond to this situation. For $A_2 = 1$ GPa, the austenite ($e_2 = 0$) is a metastable local minimum and there are two stable martensitic minima. Figure 6(a) and 6(b) show the situation for $\sigma = 0$. Since there are no nucleation mechanisms in the present simulations, the system remains in an austenite phase ($e_2 = 0$) in all the grains. Loading is simulated in exactly the same manner as for the $A_2 = -2$ case. In Figure 6(c) and Figure 6(d) we observe that a stress induced transformation has heterogeneously occurred in all the grains ($\sigma = 30.76$ MPa) (although no local stresses have been introduced in the model, the heterogeneous nucleation occurs due to the strain gradients at the grain boundaries which act as embryos for the transformation). The transformed regions are represented by yellow/red shades whereas the untransformed austenite regions are represented by light green shades. Some grains also show the presence of the unfavored variant ($e_2 < 0$) represented by dark green and blue shades. Figure 6(d) shows that at this stress level, the texture is the same as for the unloaded configuration. At the maximum stress (Figure 6(e)) $\sigma = 200$ MPa, most of the system has transformed although some austenite and the unfavored variant domains remain. As in the earlier case, grains with higher misorientation have also rotated (Figure 6(f)). Upon unloading, for this case also some of the unfavored domains reappear, as can be seen in Figure 6(g). Figure 6(h) shows that the texture returns to its preloading state.

Next, we consider the case $A_2 = 2$ GPa for which $e_2 = 0$ is the global minimum and there are two metastable martensitic minima. For this case, the ‘‘arrested’’ polycrystal exists in the

austenite phase before loading. This situation is depicted in Figure 7(a) where the strain ϵ_2 is close to zero everywhere. The corresponding orientation distribution is shown in Figure 7(b). The system is loaded at an identical loading rate as in the earlier cases. Figure 7(c) shows the spatial distribution of ϵ_2 at a load of $\sigma = 30.76$ MPa. A *stress induced* martensitic transformation from the square phase to the rectangular phase takes place heterogeneously, as can be seen from the transformed regions (yellow/red shades) that are embedded in a matrix of the untransformed austenite (green/blue shades). Figure 7(d) shows that at this stress level, the orientation distribution does not change appreciably. Upon loading further to $\sigma = 200$ MPa, the transformed phase grows although the austenite phase is locally retained in some regions (Figure 7(e)). Similar to the earlier cases, transformation accommodating grain rotations are also observed for this case, as seen in Figure 7(f). When the load is removed, the domain structure shown in Figure 7(g) is observed. Here, most of the system reverts to an austenite phase but some martensitic domains (as yellow streakings) remain giving rise to a very small residual strain. Figure 7(h) shows the corresponding orientation distribution that returns to its preloading state.

Finally, we discuss the case $A_2 = 3$ GPa which delineates a pseudoelastic behavior. The appropriate free energy shown in Figure 1 has only one minimum, corresponding to $e_2 = 0$. For this case as well, the preloading state is austenite and the strain ϵ_2 is very small everywhere, as seen in Figure 8(a). The corresponding orientation distribution is shown in Figure 8(b). Nucleation of martensitic variants in the austenite matrix can be observed in Figure 8(c), corresponding to $\sigma = 30.76$. Figure 8(d) shows that the orientation distribution associated with this stress does not change much. As the stress is further increased to $\sigma = 200$ MPa, most of the system is transformed to (stress induced) martensite, as shown in Figure 8(e). Rotations of grains with large misorientation with the loading axis are observed for this case also (Figure 8(f)). In contrast to the $A_2 = -2$ GPa and $A_2 = 2$ GPa cases, this system reverts to a homogeneous austenite phase upon unloading (Figure 8(g)), i.e. there is no residual strain. Thus, this case shows pseudoelasticity. The grain rotations are also recovered upon unloading, as seen in Figure 8(h).

We have also simulated the single crystal loading-unloading cycle corresponding to Figures 6, 7 and 8. Unlike the $A_2 = -2$ GPa case discussed in Figure 3, the system always remains in a single domain state during the loading and unloading. This is because there are no nucleation mechanisms in the single crystal cases to create twin boundaries. A stress induced martensitic transformation occurs homogeneously at a critical load, for all these cases. Upon unloading, there is no renucleation of the twinned state.

The stress-strain curves corresponding to Figures 6, 7 and 8 are depicted in Figure 9. The corresponding single crystal curves are also shown. It is clear that the residual strain decreases as the elastic constant A_2 (or the temperature) increases. It is also seen that the residual strains for the polycrystal simulations corresponding to $A_2 = 1$ GPa and $A_2 = 2$ GPa are smaller than their single crystal counterparts due to averaging over different orientations and nucleation mechanisms that exist in the polycrystal. However, for the pseudoelastic case ($A_2 = 3$ GPa), the residual strains are zero for both the single- and polycrystal cases.

IV. SUMMARY AND DISCUSSION

We have proposed a framework to study the mechanical properties of shape memory polycrystals. We have coupled the elastic free energy for a square to rectangle transition to a phase-field model describing crystal orientations. This approach can be readily extended to any crystal symmetry and does not require any a priori assumption of grain shapes or microstructure. The microstructure is governed by the crystal symmetries encoded in the appropriate elastic free energy functional. The long-range elastic interaction between the grains is also incorporated. An important feature of the present work is the coupling between the grain orientation and elasticity so that the metastability of the polycrystal may be accounted for within the same framework.

We studied mechanical properties of shape memory polycrystals and single crystals in different temperature regimes. There are significant differences between the mechanical response of single- and polycrystals. Since the mechanical properties of the polycrystal are an average of individual grains, the stress-strain curves are smoother compared to those of the single crystals. The inhomogeneities in the polycrystal ensure that domain walls influence the mechanical behavior throughout the loading-unloading process. In the temperature regimes with nonzero residual strain, the unloaded polycrystals not only have reduced strain but also show domain microstructure. In contrast, the simulated defect free single crystals exhibit no such patterns after unloading and have much higher residual strains. Our findings are consistent with the fact that in general, polycrystals have poor shape memory properties in comparison to single crystals^{3,20,21}. We emphasize that our findings apply to materials where the symmetry change due to the transformation is not particularly large and the number of low symmetry variants is relatively small (for example materials that show a cubic to tetragonal transformation). Materials such as NiTi, which undergo a cubic to monoclinic transformation have a relatively larger symmetry change and larger number of low symmetry vari-

ants. For NiTi, the differences between shape memory behavior of polycrystals and single crystals is not significant. Thus, the issues of how well strain is accommodated and how favored are the variants can play a role in determining the shape memory properties. Clearly, further investigation of this aspect is required.

The simulations also predict that grains with a large misorientation with the loading direction can undergo reversible rotations, even in the absence of plastic flow. The magnitude of the rotation is very small in the linear elastic regime and significant rotation occurs only after the transformation begins. It is well known that grains can rotate in the plastic regime to accommodate crystallographic slip²². Although there are no plastic effects within the present model, there are elastic nonlinearities that couple to the orientation degrees of freedom. Measurements of texture evolution upon loading in NiTi shape memory alloys have recently been reported²³. However, from these experiments, it is not possible to clarify if the rotational mechanism we observed exists. Our simulations suggest that for grains with a high misorientation with the loading axis, in principle, rotation as well as detwinning can occur simultaneously for shape memory polycrystals. There appears to be an underlying tendency in the polycrystal to decrease the effect of misorientations. Based on experiments and finite element simulations, a similar tendency where favorably oriented grains induce the transformation in unfavorably oriented grains, thereby effectively reducing the effect of grain misorientations, has been discussed by Gall et al⁶. Since the grain orientations are not fixed in our simulations, this reduction in the effect of misorientations can be achieved by evolution of the transformation strains as well as the grain orientations. Further experiments are needed to clarify to what extent such a mechanism indeed exists in real shape memory polycrystals. The magnitude of this grain rotation depends on the parameters of the polycrystal phase field model, or on the energy barrier between the grains. These parameters have been chosen arbitrarily for illustrative purposes in the present simulations. An estimation of these parameters from experiment or atomistic simulations will be useful for a better comparison with experiments.

ACKNOWLEDGEMENT

We are grateful to F. L. Addessio and T. O. Williams for fruitful discussions. This work was supported by the U.S. Department of Energy.

- ¹ K. Otsuka and C. M. Wayman (eds.), *Shape Memory Materials*, Cambridge University Press, Cambridge, (1998).
- ² C. M. Wayman, *Journal of Metals* **32**, 129 (1980).
- ³ K. Bhattacharya and R. V. Kohn, *Arch. Rational Mech. Anal.* **139**, 99 (1997); Y. C. Shu and K. Bhattacharya, *Acta Mater.* **46**, 5457 (1998).
- ⁴ M. Huang, X. Gao and L. C. Brinson, *International Journal of Plasticity* **16**, 1371 (2000).
- ⁵ F. Falk, *International Journal of Engineering Science* **27**, 277 (1989).
- ⁶ K. Gall, T. J. Lim, D. L. McDowell, H. Sehitoglu and Y. I. Chumlyakov, *International Journal of Plasticity* **16**, 1189 (2000).
- ⁷ Y. M. Jin, A. Artemev and A. G. Khachaturyan, *Acta Mater.* **49**, 2309 (2001); A. Artemev, Y. M. Jin and A. G. Khachaturyan, *Philos. Mag. A* **82**, 1249 (2002).
- ⁸ B. Morin, K. R. Elder, M. Sutton and M. Grant, *Phys. Rev. Lett.* **75**, 2156 (1995).
- ⁹ L. Q. Chen and W. Yang, *Phys. Rev. B* **50**, 15752 (1994).
- ¹⁰ J. A. Warren, W. C. Carter and R. Kobayashi, *Physica (Amsterdam)* **261A**, 159 (1998).
- ¹¹ F. Falk, *Acta Metallurgica* **28**, 1773 (1980).
- ¹² G. R. Barsch and J. A. Krumhansl, *Phys. Rev. Lett.* **53**, 1069 (1984).
- ¹³ S. R. Shenoy, T. Lookman, A. Saxena and A. R. Bishop, *Phys. Rev. B* **60**, R12537 (1999).
- ¹⁴ K. Ø. Rasmussen, T. Lookman, A. Saxena, A. R. Bishop, R. C. Albers and S. R. Shenoy, *Phys. Rev. Lett.* **87**, 055704 (2001).
- ¹⁵ T. Lookman, S. R. Shenoy, K. Ø. Rasmussen, A. Saxena and A. R. Bishop, *Phys. Rev. B* **67**, 024114 (2003).
- ¹⁶ S. H. Curnoe and A. E. Jacobs, *Phys. Rev. B* **64**, 064101 (2001).
- ¹⁷ S. Kartha, J. A. Krumhansl, J. P. Sethna and L. K. Wickham, *Phys. Rev. B* **52**, 803 (1995); G. R. Barsch and J. A. Krumhansl, *Proc. ICOMAT-92, Eds. C. M. Wayman and J. Perkins, Monterey Institute for Advanced Studies, Monterey, CA, 1993, pp.53-64.*

- ¹⁸ E. A. H. Love, *A treatise on the mathematical theory of elasticity* (Dover, New York, 1944).
- ¹⁹ S. Muto, R. Oshima and F. E. Fujita, *Acta Metallurgica et Materialia* **38**, 685 (1990).
- ²⁰ K. Enami, V. V. Martynov, T. Tomie, L. G. Khandros, and S. Nenno, *Trans. Japan Inst. Metals* **22**, 357 (1981).
- ²¹ Y. D. Kim and C. M. Wayman, *Metall. Trans.* **23A**, 2981 (1992).
- ²² L. Marguiles, G. Winther and H. F. Poulsen, *Science* **291**, 2392 (2001).
- ²³ R. Vaidyanathan, M. A. M. Bourke and D. C. Dunand, *Acta Mater.* **47**, 3353 (1999).

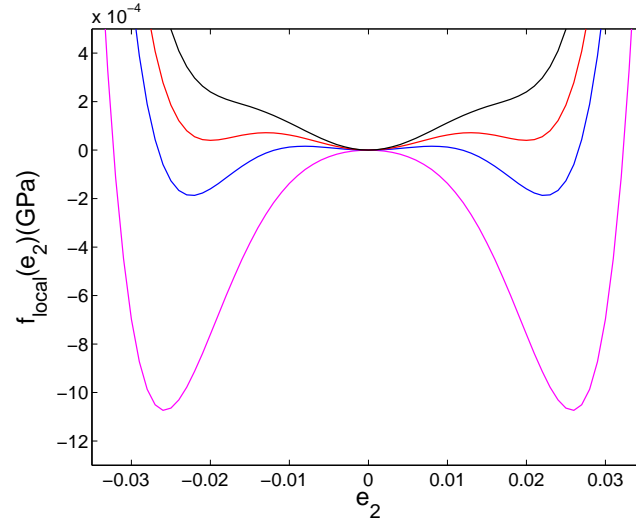


FIG. 1: Local free energy density vs. e_2 as a function of temperature. The relatively high temperature (black curve) has $A_2 = 3$ GPa, and successive curves with decreasing temperatures are for $A_2 = 2, 1$ and -2 GPa, respectively.

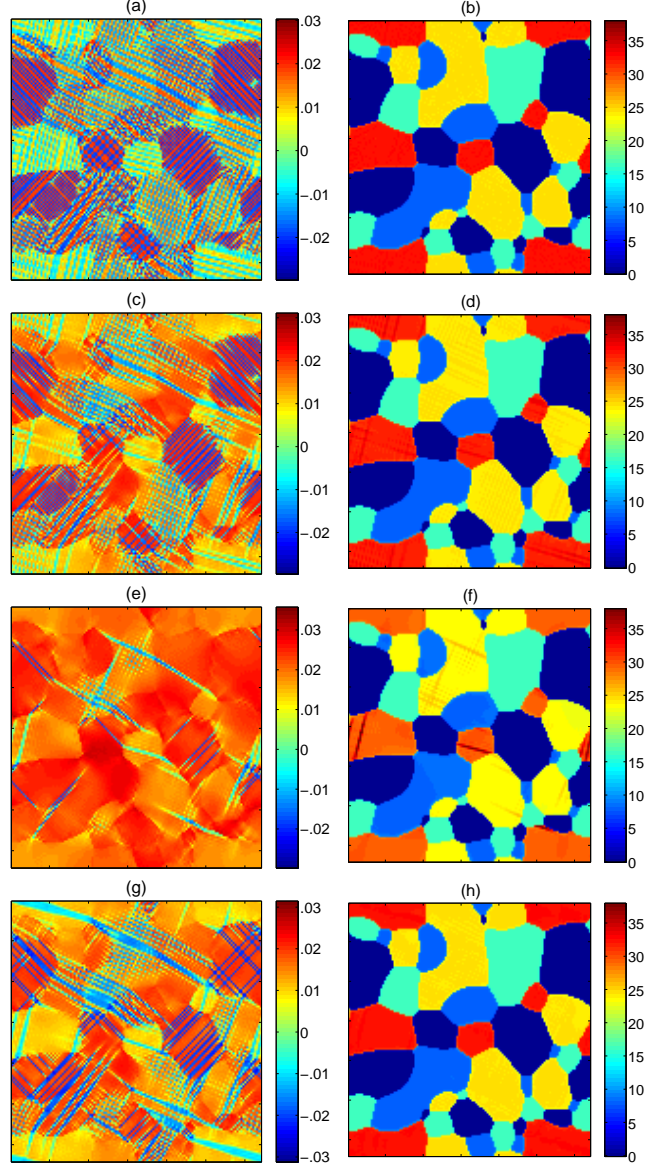


FIG. 2: Spatial distribution of $\epsilon_2(\vec{r})$ (deviatoric strain in a global frame) for a polycrystal with $A_2 = -2$ GPa (snapshots (a),(c),(e) and (g)) and $\theta(\vec{r})$ in degrees (snapshots (b),(d),(f) and (h)). The corresponding stress levels are $\sigma = 0$ (before loading, (a) and (b)), $\sigma = 46.15$ MPa ((c) and (d)), $\sigma = 200$ MPa ((e) and (f)) and $\sigma = 0$ (after unloading, (g) and (h)).

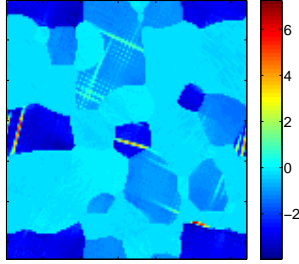


FIG. 3: Spatial distribution of $\Delta\theta = \theta(\sigma) - \theta(\sigma = 0)$ in degrees for $\sigma = 200$ MPa (corresponding to Figure 2(f)).

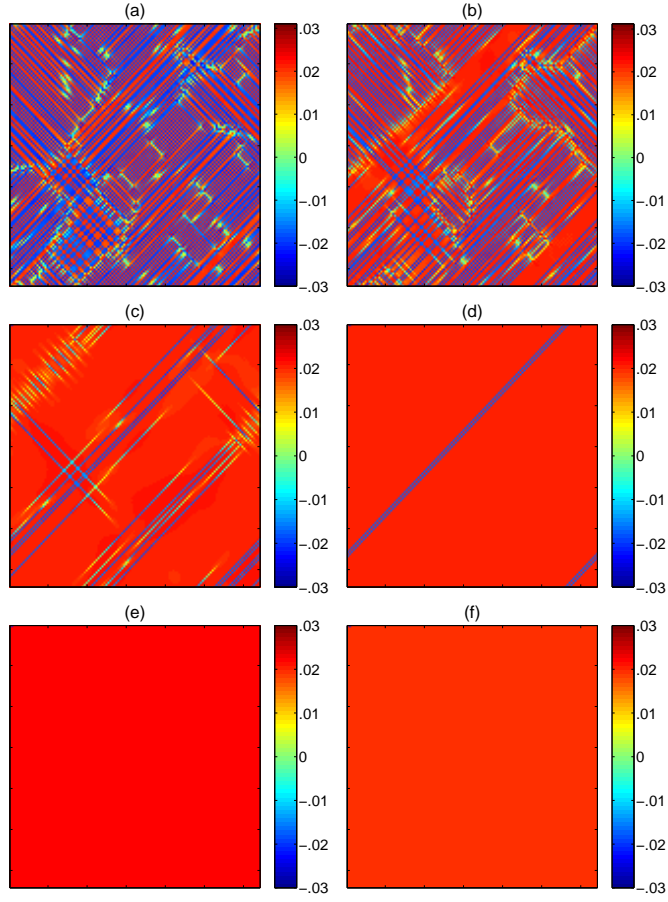


FIG. 4: Spatial distribution of $\epsilon_2(\vec{r})$ (deviatoric strain in a global frame) for a single crystal ($\theta(\vec{\eta}) = 0^\circ$) with $A_2 = -2$ GPa. The corresponding stress levels are $\sigma = 0$ (before loading) (a), $\sigma = 46.15$ MPa (b), $\sigma = 56.41$ MPa (c), $\sigma = 71.79$ MPa (d), $\sigma = 200$ MPa (e) and $\sigma = 0$ (after unloading) (f).

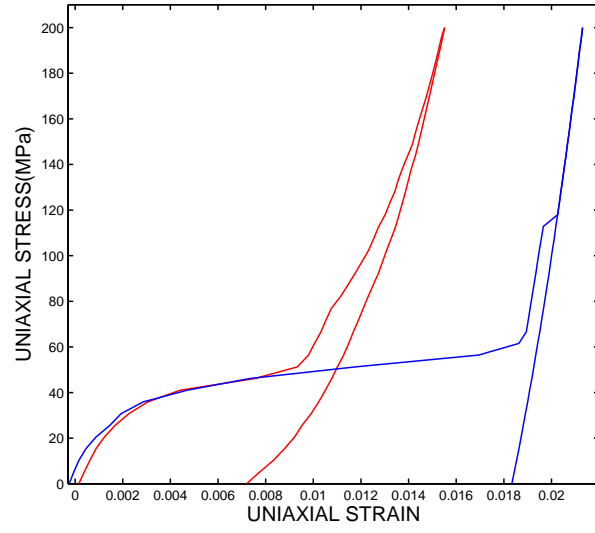


FIG. 5: Variation of applied load σ with average uniaxial strain $\langle \epsilon_{xx} \rangle$ for $A_2 = -2$ GPa for a polycrystal (red curve) and a single crystal (blue curve).

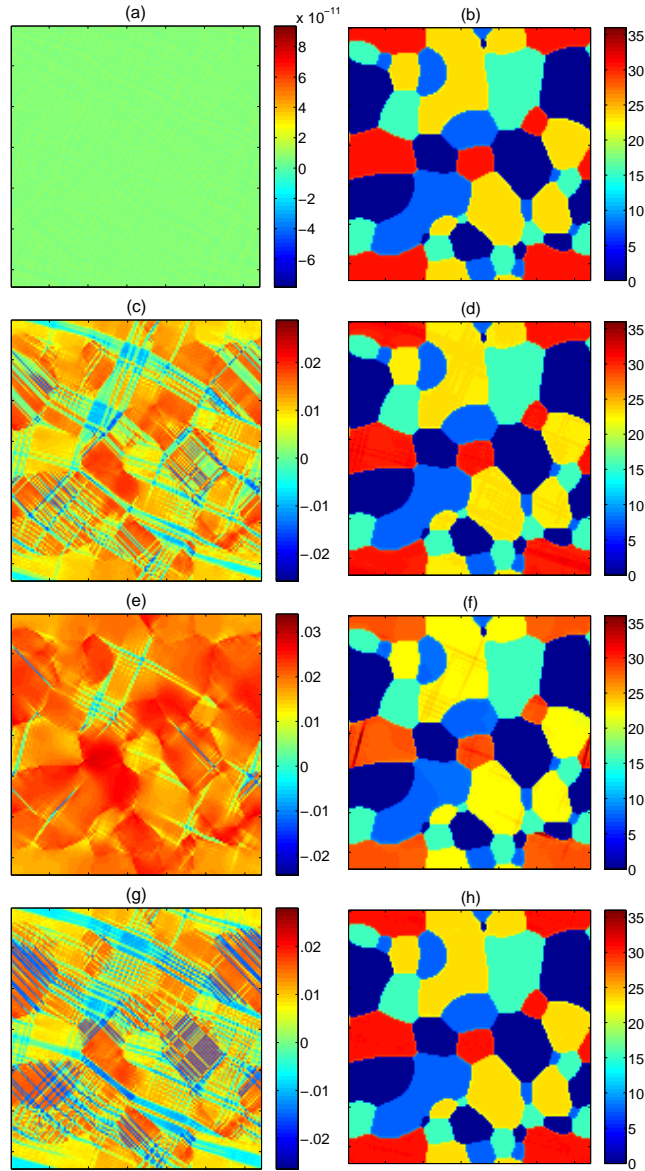


FIG. 6: Spatial distribution of $\epsilon_2(\vec{r})$ (deviatoric strain in a global frame) for a polycrystal with $A_2 = 1$ GPa (snapshots (a),(c),(e) and (g)) and $\theta(\vec{r})$ (snapshots (b),(d),(f) and (h)). The corresponding stress levels are $\sigma = 0$ (before loading, (a) and (b)), $\sigma = 30.76$ MPa ((c) and (d)), $\sigma = 200$ MPa ((e) and (f)) and $\sigma = 0$ (after unloading, (g) and (h)).

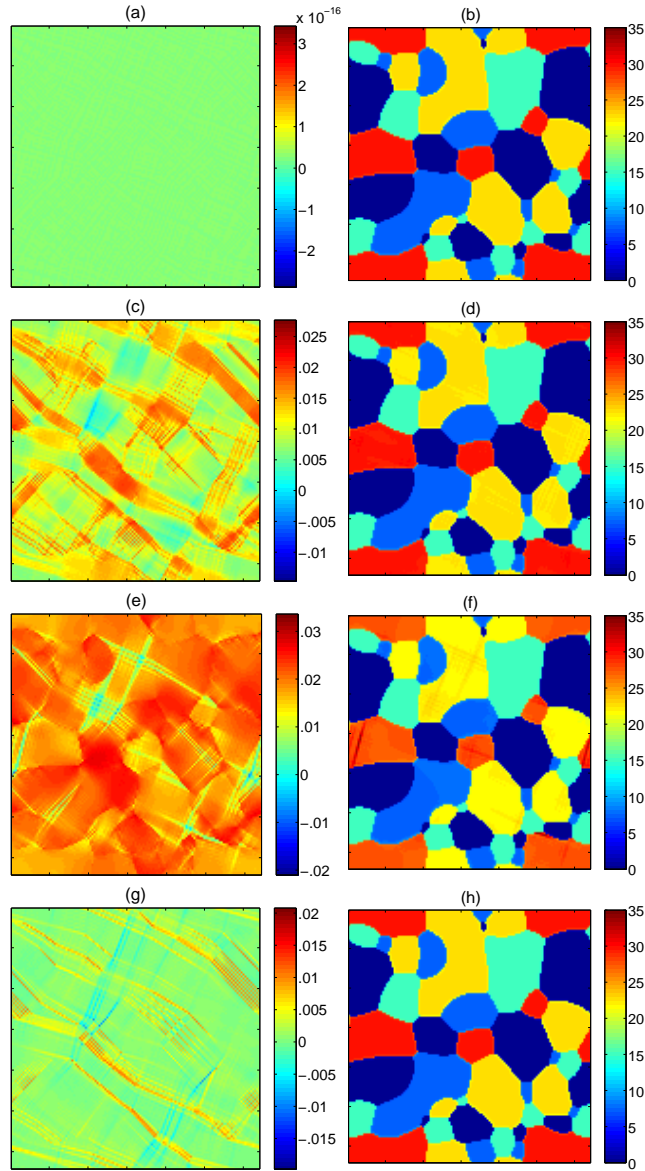


FIG. 7: Spatial distribution of $\epsilon_2(\vec{r})$ (deviatoric strain in a global frame) for a polycrystal with $A_2 = 2$ GPa (snapshots (a),(c),(e) and (g)) and $\theta(\vec{r})$ in degrees (snapshots (b),(d),(f) and (h)). The corresponding stress levels are $\sigma = 0$ (before loading, (a) and (b)), $\sigma = 30.76$ MPa ((c) and (d)), $\sigma = 200$ MPa ((e) and (f)) and $\sigma = 0$ (after unloading, (g) and (h)).

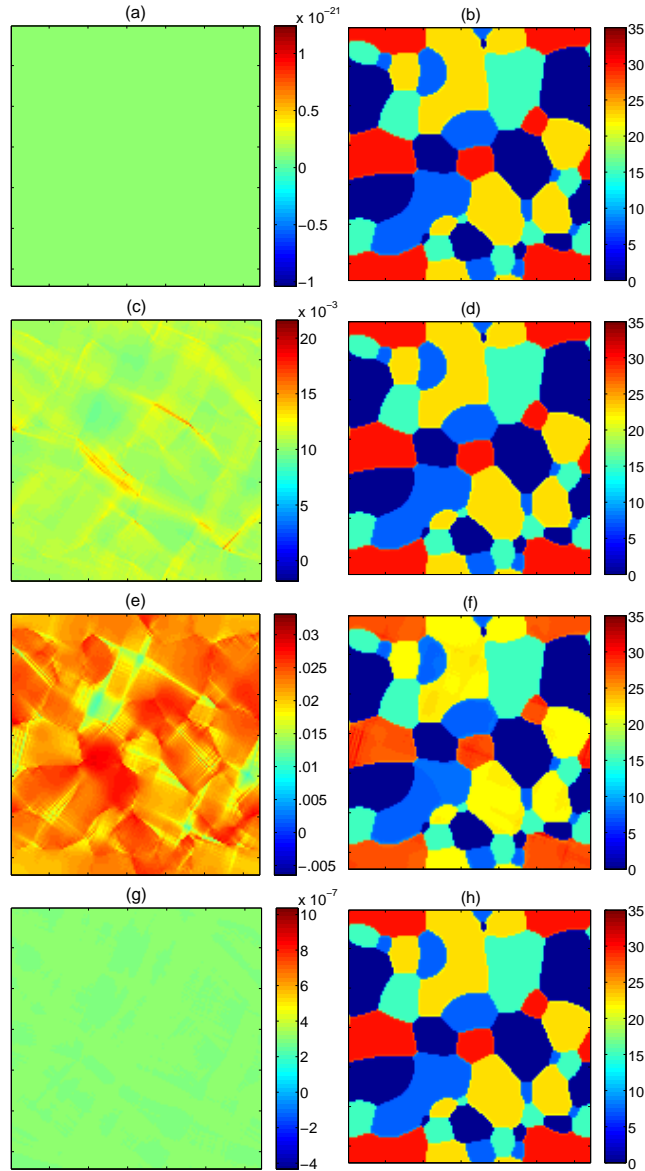


FIG. 8: Spatial distribution of $\epsilon_2(\vec{r})$ (deviatoric strain in a global frame) for a polycrystal with $A_2 = 3$ GPa (snapshots (a),(c),(e) and (g)) and $\theta(\vec{r})$ in degrees (snapshots (b),(d),(f) and (h)). The corresponding stress levels are $\sigma = 0$ (before loading, (a) and (b)), $\sigma = 30.76$ MPa ((c) and (d)), $\sigma = 200$ MPa ((e) and (f)) and $\sigma = 0$ (after unloading, (g) and (h)).

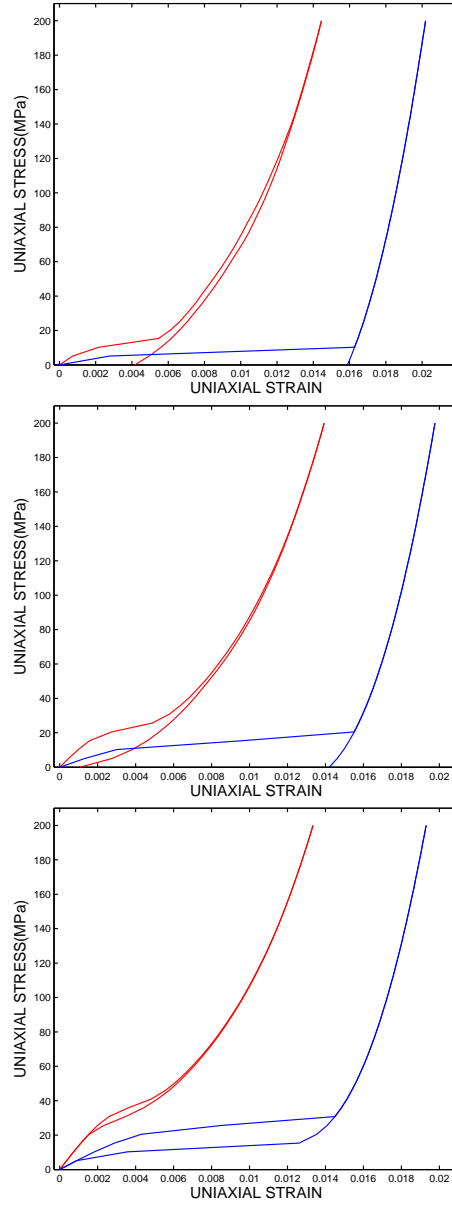


FIG. 9: Variation of applied load σ vs. average uniaxial strain $\langle \epsilon_{xx} \rangle$ as a function of (increasing) temperature. From top to bottom, $A_2 = 1, 2, 3$ GPa, respectively. Red curves correspond to a polycrystal and blue curves to a single crystal.